# Theoretical Study on the Electronic Configurations and Nature of Chemical Bonds of Dirhodium Tetraacetato Complexes $[Rh_2(CH_3COO)_4(L)_2]$ (L = $H_2O$, Free): Broken Symmetry Approach

**Yusuke Kataoka,*[1] Yasutaka Kitagawa,[1] Toru Saito,[1] Yasuyuki Nakanishi,[1] Toru Matsui,[1] Konomi Sato,[2] Yuhei Miyazaki,[2] Takashi Kawakami,[1] Mitsutaka Okumura,[1] Wasuke Mori,[2] and Kizashi Yamaguchi[3]**

[1]Department of Chemistry, Graduate School of Science, Osaka University, Machikaneyama-cho, Toyonaka, Osaka 560-0043

[2]Department of Chemistry, Faculty of Science, Kanagawa University, Tsuchiya, Hiratsuka, Kanagawa 259-1293

[3]Department of Materials Engineering Science, Graduate School of Engineering Science, Osaka University, Toyonaka, Osaka 560-8531

Received April 30, 2010; E-mail: kataoka@chem.sci.osaka-u.ac.jp

The electronic configurations and the nature of chemical bonds of the classical *lantern*-type dinuclear rhodium(II) tetraacetato complexes $[Rh_2(CH_3COO)_4(L)_2]$ (L = $H_2O$, free) have been carefully investigated with broken symmetry (BS) Hartree–Fock (HF), BS density functional theory (DFT), and BS hybrid DFT (HDFT) methods. Several electronic configurations have been proposed for the ground states of the $[Rh_2(RCOO)_4(H_2O)_2]$ complexes. In this study, we concluded that those different electronic configurations originate from the position of the axial $H_2O$s, and not along the Rh–Rh length. The BS(U)B3LYP calculation indicates that the stability of the $\sigma$ and $\delta$ orbitals changed when the Rh–$OH_2$ length was 2.35 Å. The natural orbital (NO) analyses and chemical indices clearly indicate that there is a $\sigma$-type single bond between the Rh ions, and that the axial $H_2O$s does not affect the overlap.

Dirhodium(II) tetrakis(carboxylato) complexes, $[Rh_2(RCOO)_4(L)_2]$, are extremely important in terms of their utilization as supramolecular building blocks, antitumor drugs, catalysts for carbenoid insert reactions, and so on.[1–3] The Rh–Rh distance of a typical dirhodium tetrakis(carboxylato) complex, $[Rh_2(CH_3COO)_4(H_2O)_2]$ (Figure 1), is 2.386 Å; therefore, it has been considered that there is a single bond between the Rh ions.[4] For the past several decades, the electronic configurations of the dirhodium tetrakis(carboxylato) complexes have been theoretically examined using various calculation methods. These results have led to the conclusion that the Rh ions have a single bond, which consists of $\sigma^2\pi^4\delta^2\delta^{*2}\pi^{*4}$ in the singlet ground state (We note that the word "configuration" used here has a meaning of both the orbital occupation and the ordering of orbital energies.). However, other configurations have also been proposed. For example, Dubicki and Martin performed extended Hückel calculations on $[Rh_2(CH_3COO)_4(H_2O)_2]$ and concluded that the electronic configuration was $\pi^4\sigma^2\delta^2\delta^{*2}\pi^{*4}$.[5] On the other hand, Norman and Kolari carried out SCF X$\alpha$SW calculations for $[Rh_2(HCOO)_4(L)_2]$ (L = free, $H_2O$) and reported that the open-shell electronic configurations $\sigma^2\pi^4\delta^2\pi^{*4}\delta^{*2}$ were stable.[6] The earliest report of ab initio calculation was presented by Nakatsuji et al. They performed the RHF calculations for $[Rh_2(HCOO)_4(L)_2]$ (L = free, $H_2O$) and the obtained electronic configurations were $\pi^4\delta^2\pi^{*4}\delta^{*2}\sigma^2$.[7] In 2000, Lichtenberger and Cotton reported calculated results of the pure DFT (RBLYP) method on $[Rh_2(CF_3COO)_4]$ and found that the electronic configuration was $\sigma^2\pi^4\delta^2\delta^{*2}\pi^{*4}$.[8] Very recently, Sizova et al. reported that the calculated results of the hybrid DFT (RB3LYP) method on $[Rh_2(HCOO)_4(L)_2]$ (L = free, $H_2O$) indicated configurations of $\sigma^2\pi^4\delta^2\pi^{*4}\delta^{*2}$ and $\delta^2\pi^4\sigma^2\pi^{*4}\delta^{*2}$, respectively.[9] In addition to those results, some different electronic configurations have also been reported from calculations using other functional sets on related complexes.[10] However, the electronic configurations of the dirhodium

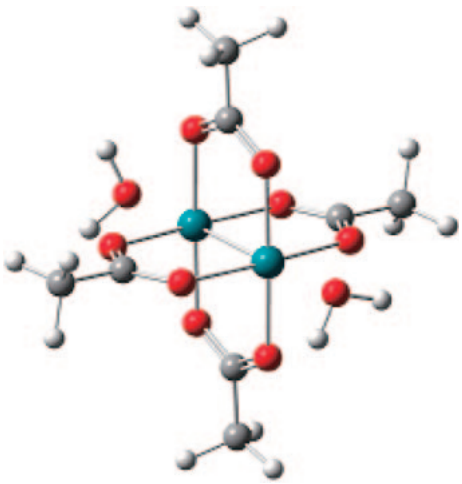

**Figure 1.** Molecular structure of $[Rh_2(CH_3COO)_4(H_2O)_2]$.

Published on the web November 27, 2010; doi:10.1246/bcsj.20100128

tetrakis(carboxylato) complexes have not been clarified yet. Because the determination of the electronic configurations are necessary for further understanding of their properties, it is meaningful to attain the electron configurations of the dirhodium tetrakis(carboxylato) complexes by theoretical calculations.[11] In this paper, we investigate the electronic configurations and the nature of chemical bonds between the $Rh^{II}$ ions of the typical dirhodium tetrakis(carboxylato) complexes, $[Rh_2(CH_3COO)_4(L)_2]$ (L = free, $H_2O$), by using the broken-symmetry (BS)-HF, the BS-DFT, and the BS-HDFT methods. The relation between structural parameters and electronic configurations are specifically examined by using X-ray and optimized geometries.

## Theoretical Background

**Computational Details.** All ab initio calculations are performed using the LANL2DZ basis set for Rh atoms, and 6-31G** basis set for ligands. In order to correct the static correlation, a spin-unrestricted, i.e., BS, method is employed for the open-shell singlet calculations. In addition, three types of DFT functional sets that have different ratio of the Hartree–Fock exchange (B3LYP, BHandHLYP, and BLYP) are examined, as well as the pure HF method on Gaussian 03 and 09 (especially for CAM-B3LYP)[16] program packages.[12] For the model structure of the $Rh_2$ complex, many people have used a reduced ligand, i.e., $HCOO^-$, as a substitution for $CH_3COO^-$, although the X-ray (crystal) structure of $[Rh_2(HCOO)_4(H_2O)_2]$ has not been obtained. In order to avoid any error from the reduction of the ligand, we use a realistic $[Rh_2(CH_3COO)_4(H_2O)_2]$ complex with a known geometry that has been analyzed experimentally. We carried out a geometry optimization of the complex, starting with the initial geometry of the X-ray crystallographic data. For a comparative study, the geometry of the without-axial-ligand-model i.e., $[Rh_2(CH_3COO)_4]$ is also optimized, because its X-ray structure is not determined.

**Natural Orbital Analysis.** Because the BS method does not provide a conventional molecular orbital diagram, we performed a natural orbital (NO) analysis to investigate their chemical bonds. In addition, the occupation numbers provide very useful information about the Rh–Rh bond, such as the overlap between the $\alpha$ and $\beta$ orbitals, and the contribution of the double excitation to the ground state. Yamaguchi has proposed a procedure to analyze the chemical bond using the occupation number. Because it can be related to the weight of the double excitation state in the chemical bond, one can utilize the occupation number to analyze the instability in the chemical bond.[13] The NOs are determined by diagonalizing the first-order density matrices as

$$\rho(r, r') = \sum n_i \{\phi_i(r)\}^* \phi_i(r') \quad (1)$$

where $n_i$ denotes the occupation number of the NO $\phi_i$. If an occupation number is close to 1.0, then the two electrons are largely localized on each Rh ion.[14] On the other hand, $n_i$ should be equal to 2.0 if a stable chemical bond exists. One of the merits of the NOs is that they give us a symmetry-adapted (SA)-like orbital picture based on the DODS approach.[14] To assess the instability in the Rh–Rh bond, the instability value $y_i$ is introduced here as follows:

$$y_i = 2W_D{}^2 = \frac{n_i{}^2 - 4n_i + 4}{n_i{}^2 - 2n_i + 2} \quad (2)$$

where $n_i$ denotes the occupation number of the highest-occupied NO (HONO), and $W_D$ is the weight of a double excitation for the corresponding orbital. The effective bond order is given by

$$b_i = \frac{n_i - n_i^*}{2} \quad (3)$$

where $n_i{}^*$ denotes the occupation number of lowest-unoccupied NO (LUNO).

## Results and Discussion

**Electronic Configuration and Rh–Rh Interaction of $[Rh_2(CH_3COO)_4(H_2O)_2]$.** In order to examine the electronic configurations of the $Rh_2$ complexes, we began with the calculations of the real complex, $[Rh_2(CH_3COO)_4(H_2O)_2]$. As explained above, we carried out the geometry optimization by using the initial geometry of the X-ray data. Although it has been reported that the optimization of $[M_2(RCOO)_4(H_2O)_2]$ slightly shifts the axial $H_2O$ from the M–M axial axis, there have been no reports on how the $H_2O$-shift changes the electronic configuration of the complex.[15] The fact that many possible electronic configurations of $[Rh_2(RCOO)_4(H_2O)_2]$ have been reported seems to suggest that the shift of $H_2O$ from the Rh–Rh axial axis may change the configuration. For that reason, we initially compared the electronic configurations of the X-ray geometry with that of the optimized geometry using the UB3LYP method. The optimized structural parameters, total energies, and $\langle S^2 \rangle$ (total spin angular momentum) values are summarized in Tables 1 and 2.

As shown in Table 1, the optimized geometries are almost in agreement with the X-ray geometry of $[Rh_2(CH_3COO)_4(H_2O)_2]$, except for the $H_2O$ ligands on the axial axis. The optimized Rh–$OH_2$ distance is longer than that of the X-ray geometry by about 0.1 Å. In the geometry optimization, the calculated total energy is slightly more stabilized (7.42 kcal mol$^{-1}$) than that of the X-ray geometry. The estimated binding energies of the Rh–$OH_2$ are 17.7 and 14.8 kcal mol$^{-1}$ for the optimized and X-ray geometries, respectively. Because the difference in the Rh–$OH_2$ binding energies between the two geometries is about 3 kcal mol$^{-1}$, we conclude that the stabilization energy mainly comes from the reorientation of the $H_2O$.

We also investigated the dependence of the optimized structures on the calculation methods. As shown in Table 1, the optimized geometries using the UBLYP and UBHandHLYP

**Table 1.** Optimized Geometry of $[Rh_2(CH_3COO)_4(H_2O)_2]$ (Distance/Å, Angle/°)

| | UHF | UBHandHLYP | UB3LYP | UBLYP | Exp. |
|---|---|---|---|---|---|
| Rh–Rh | 2.588 | 2.413 | 2.409 | 2.433 | 2.386 |
| Rh–O (bridge) | 2.099 | 2.058 | 2.077 | 2.099 | 2.042 |
| Rh–O (axial) | 2.459 | 2.376 | 2.407 | 2.445 | 2.309 |
| O···O | 2.221 | 2.238 | 2.269 | 2.300 | 2.246 |
| OCO | 125.7 | 125.8 | 126.1 | 125.5 | 124.5 |
| RhRhO (bridge) | 84.27 | 86.71 | 87.38 | 87.66 | 87.70 |
| RhRhO (axial) | 168.6 | 171.6 | 172.7 | 173.3 | 176.5 |

**Table 2.** Electronic Configurations, HOMO–LUMO Gaps, $\langle S^2 \rangle$ Values, and Total Energies of $[Rh_2(CH_3COO)_4(H_2O)_2]$

| Functional | Geometry | Electronic configuration | $\lvert\Delta E_{(LUMO-HOMO)}\rvert$/eV | $\langle S^2 \rangle$ | Total energy/au |
|---|---|---|---|---|---|
| UHF | X-ray | $\delta^2\pi^4\sigma^2\pi^{*4}\delta^{*2}$ | 12.1 | 0.6787 | −1287.5071 |
| | Optimize | $\delta^2\sigma^2\pi^4\pi^{*4}\delta^{*2}$ | 12.9 | 0.8477 | −1278.5479 |
| UBHandHLYP | X-ray | $\pi^4\delta^2\sigma^2\pi^{*4}\delta^{*2}$ | 7.45 | 0.1234 | −1285.1394 |
| | Optimize | $\delta^2\pi^4\sigma^2\pi^{*4}\delta^{*2}$ | 7.41 | 0.2043 | −1285.1537 |
| UB3LYP | X-ray | $\pi^4\delta^2\sigma^2\pi^{*4}\delta^{*2}$ | 4.19 | 0.0000 | −1286.0065 |
| | Optimize | $\pi^4\sigma^2\delta^2\pi^{*2}\delta^{*2}\pi^{*2}$ | 3.98 | 0.0001 | −1286.0183 |
| UBLYP | X-ray | $\sigma^2\pi^4\delta^2\delta^{*2}\pi^{*4}$ | 2.11 | 0.0000 | −1285.5912 |
| | Optimize | $\sigma^2\pi^4\delta^2\delta^{*2}\pi^{*4}$ | 1.80 | 0.0000 | −1285.6123 |

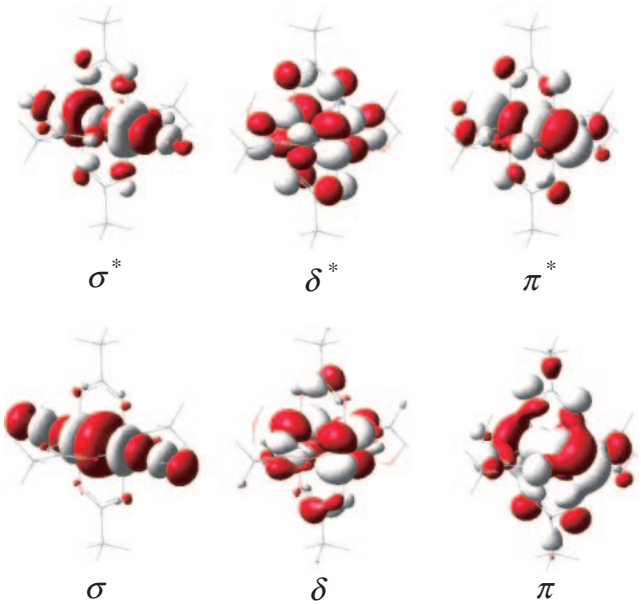


**Figure 2.** Bonding and antibonding molecular orbital of $[Rh_2(CH_3COO)_4(H_2O)_2]$ (X-ray geometry).

methods are also in good agreement with the X-ray and UB3LYP geometries of $[Rh_2(CH_3COO)_4(H_2O)_2]$, except for the Rh–$OH_2$ length. On the other hand, the UHF method elongates the Rh–Rh and the Rh–$OH_2$ lengths. These results indicate that all the methods overestimate the Rh–$OH_2$ length. These differences between the optimized and X-ray geometries in the Rh–$OH_2$ length are considered to originate mainly from the effects of the crystal packing. The Kohn–Sham orbitals of $[Rh_2(CH_3COO)_4(H_2O)_2]$ calculated with the UB3LYP method are shown in Figure 2.

As shown in Figure 2, the interaction between the $Rh^{II}$ ion and O atom of the $H_2O$ molecule occurs only in the Rh ($\sigma$) or Rh ($\sigma^*$) orbital and the lone pair orbital of $H_2O$; the other metal orbitals do not interact with the $H_2O$.

The order of orbital energies of the occupied orbitals and HOMO–LUMO gaps of $[Rh_2(CH_3COO)_4(H_2O)_2]$ of each geometry are shown in Table 2 and Figure 3.

As expected, the obtained electronic configurations (orbital energy orders) are changed by the geometries. In the case of the X-ray geometry, the electronic configuration calculated by the UB3LYP method becomes $\pi^4\delta^2\sigma^2\pi^{*4}\delta^{*2}$ and the $\sigma$ orbital is destabilized in comparison with the electronic configuration of the without-$H_2O$ model, $[Rh_2(CH_3COO)_4]$, as explained below. On the other hand, the optimized geometry produces the orbital energy order of $\pi^4\sigma^2\delta^2\pi^{*2}\delta^{*2}\pi^{*2}$ in which the $\sigma$ orbital is stabilized. The degenerate $\pi^*$ orbitals are divided into two degenerate states by the shift of the $H_2O$ position.

The calculated electronic configurations also depend on the DFT functional sets. For the UBLYP method, an orbital interchange between the $\sigma$ orbital and the other orbitals does not occur, even if the geometry is optimized, because the $\sigma$ orbital is stable. On the other hand, the orbital order of the UBHandHLYP method is the same as that of the UB3LYP method if X-ray geometry is used. However, the optimized geometry changes the stability of the $\sigma$ and $\pi$ orbitals and, consequently, the orbital orders of the UB3LYP and UBHandHLYP methods turn out to be different. Interestingly, the geometry optimization using the UHF method significantly unstabilizes the $\pi$ orbital. It is considered that the characteristics of the HF method are reflected in these hybrid DFT methods, as discussed later.

**Electronic Configuration and Rh–Rh Interaction of $[Rh_2(CH_3COO)_4]$.** For a comparative study, the relation between the optimized geometry and the electronic configuration was also investigated on the without-axial-ligand model, $[Rh_2(CH_3COO)_4]$. It is well known that some theoretical calculations have deduced that $[Rh_2(RCOO)_4]$ has the electronic configuration of $\sigma^2\pi^4\delta^2\pi^{*4}\delta^{*2}$.

First, we optimized the geometry of the ground state of $[Rh_2(CH_3COO)_4]$ with the UB3LYP method (Table 3).

As shown in Table 3, the optimized Rh–Rh length of $[Rh_2(CH_3COO)_4]$ is shorter than that of $[Rh_2(CH_3COO)_4(H_2O)_2]$, although the $CH_3COO^-$ ligands of $[Rh_2(CH_3COO)_4]$ change only slightly with the optimization. The obtained electronic configurations of $[Rh_2(CH_3COO)_4]$ are summarized in Table 4 and Figure 3. The calculated molecular orbitals of $[Rh_2(CH_3COO)_4]$ derived by the UB3LYP method are also shown in Figure 4.

The electronic configuration of $[Rh_2(CH_3COO)_4]$ calculated by the UB3LYP method is $\sigma^2\pi^4\delta^2\pi^{*4}\delta^{*2}$ and the orbital ordering is the same as those reported. However, as shown in Figure 3c, the orbital energies of $[Rh_2(CH_3COO)_4]$ are degenerate, so it is expected that the orbital order would be easily changed by the calculation method or the structural change. Therefore, we examined the dependence of the electronic configurations of $[Rh_2(CH_3COO)_4]$ on the calculation methods and the optimized geometries. The optimized geometries and the electronic configurations of $[Rh_2(CH_3COO)_4]$ for the different calculation methods are summarized in Tables 3 and 4, respectively.

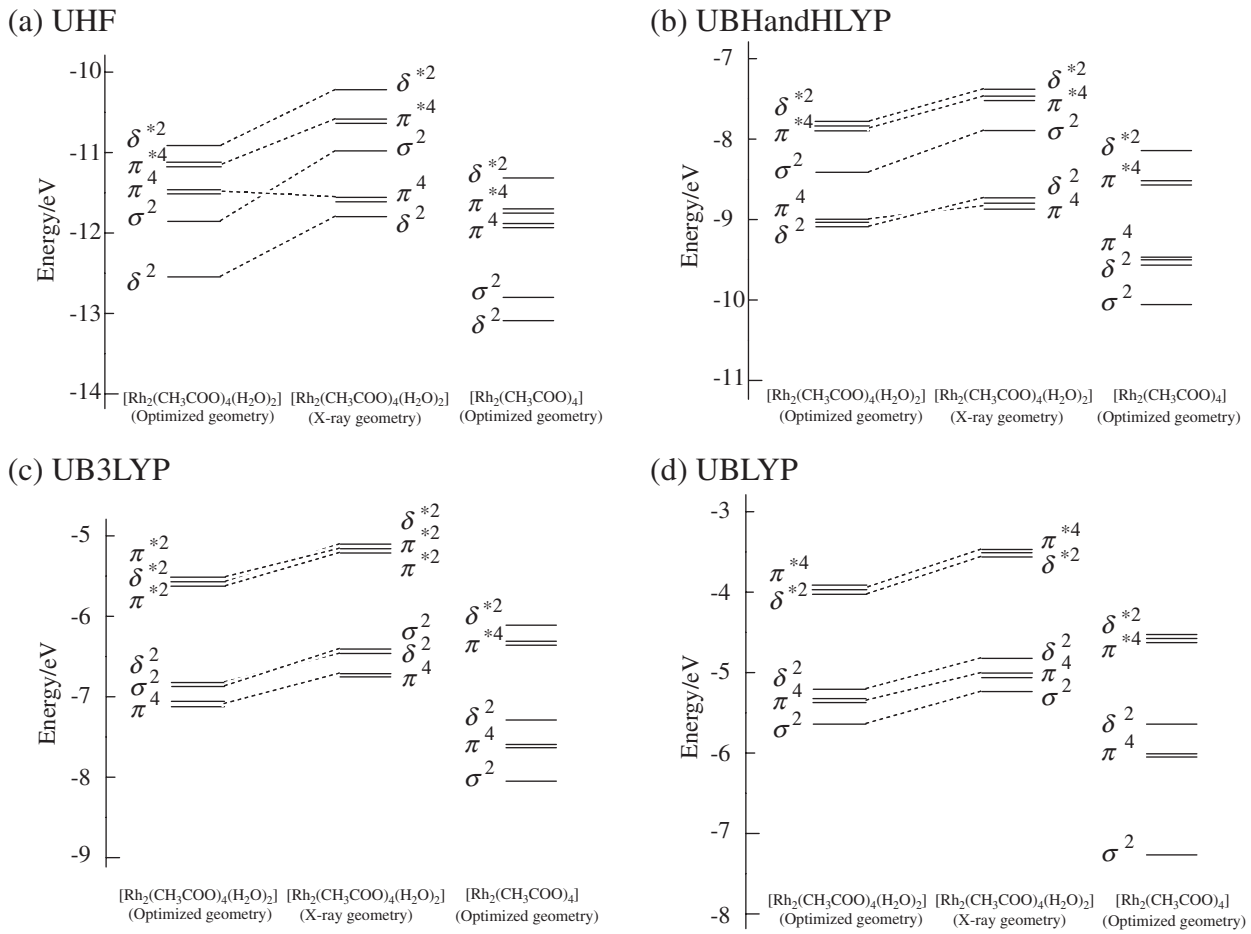


**Figure 3.** Occupied molecular orbital diagram of $[Rh_2(CH_3COO)_4(L)_2]$ (L = $H_2O$, free) (a) UHF, (b) UBHandHLYP, (c) UB3LYP, and (d) UBLYP.

**Table 3.** Optimized Geometries of $[Rh_2(CH_3COO)_4]$ (Distance/Å, Angle/°)

| | UHF | UBHandHLYP | UB3LYP | UBLYP |
|---|---|---|---|---|
| Rh–Rh | 2.571 | 2.397 | 2.389 | 2.413 |
| Rh–O (bridge) | 2.085 | 2.048 | 2.064 | 2.090 |
| O···O | 2.221 | 2.237 | 2.267 | 2.299 |
| OCO | 125.5 | 125.5 | 125.8 | 126.2 |
| RhRhO (bridge) | 85.12 | 87.71 | 88.25 | 88.35 |
| RhRhO (axial) | — | — | — | — |

**Table 4.** Electronic Configurations and HOMO–LUMO Gaps of $[Rh_2(CH_3COO)_4]$

| Functional | Geometry | Electronic configuration | $\lvert\Delta E_{(HOMO-LUMO)}\rvert$ /eV |
|---|---|---|---|
| UHF | Optimize | $\delta^2\sigma^2\pi^4\pi^{*4}\delta^{*2}$ | 12.6 |
| UBHandHLYP | Optimize | $\sigma^2\delta^2\pi^4\pi^{*4}\delta^{*2}$ | 6.26 |
| UB3LYP | Optimize | $\sigma^2\pi^4\delta^2\pi^{*4}\delta^{*2}$ | 3.00 |
| UBLYP | Optimize | $\sigma^2\pi^4\delta^2\pi^{*4}\delta^{*2}$ | 1.04 |

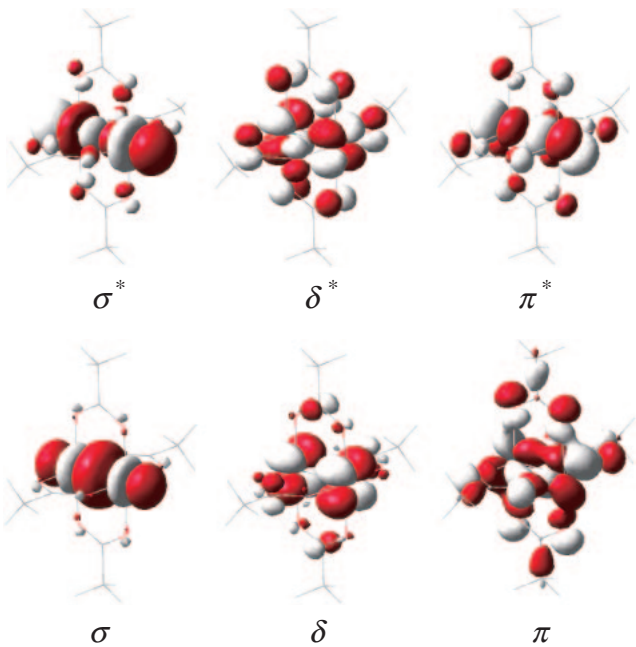


**Figure 4.** Bonding and antibonding molecular orbital of $[Rh_2(CH_3COO)_4]$.

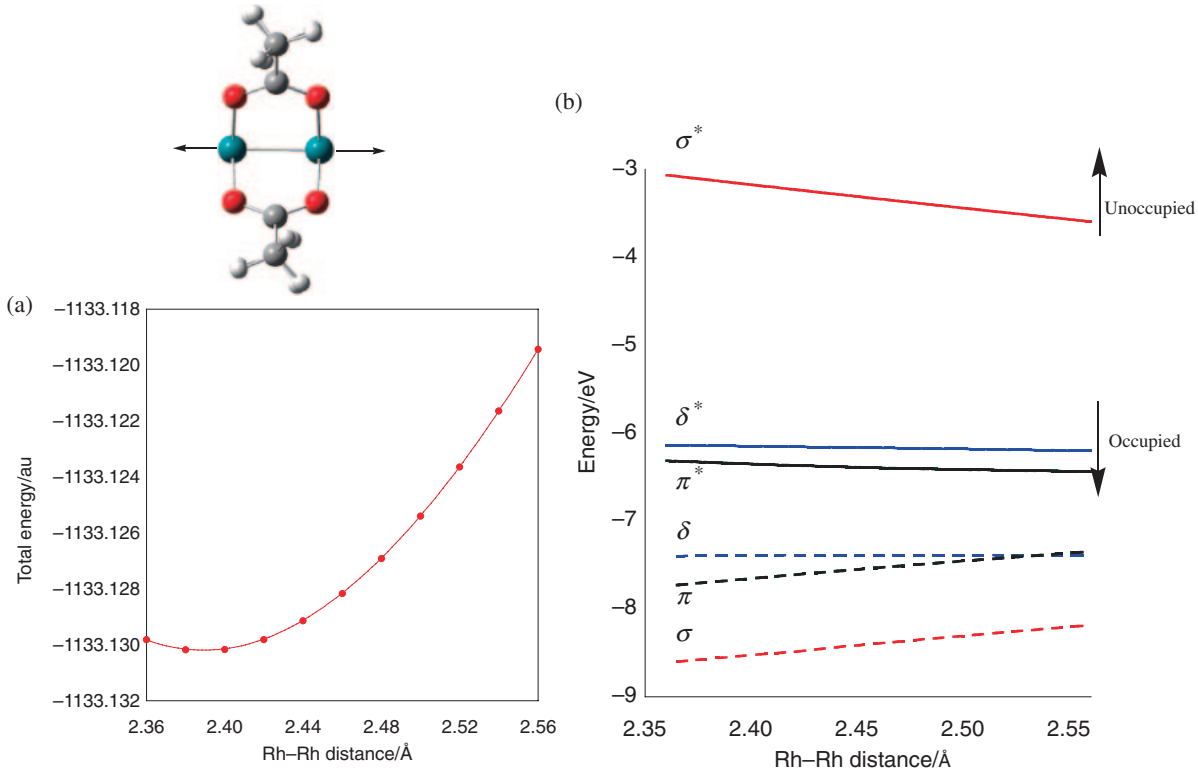


**Figure 5.** UB3LYP calculation of (a) total potential energy surface and (b) molecular orbital diagrams dependence on Rh–Rh length in $[Rh_2(CH_3COO)_4]$.

As summarized in Table 3, the optimized Rh–Rh lengths are significantly different when derived by the various methods, in comparison with the other structural parameters, however, a dependency on the methods is not clarified. On the other hand, the calculated HOMO–LUMO gaps ($|\Delta E$(HOMO–LUMO|) depend on the ratio of the HF exchange, as reported in many papers.

The calculated results show different electron configurations stemming from the different methods. The UBLYP and the UB3LYP methods give a stable $\sigma$ orbital but the UBHandHLYP method, which involves 50% HF exchange potential, unstabilizes the $\sigma$ orbital and destabilized the $\delta$ orbital. The difference seems to be closely related to the difference in optimized Rh–Rh length. For example, in the case of the UHF method, the Rh–Rh distance is elongated and it affects to stabilities of the $\sigma$ and the $\delta$ orbitals. In this way, the order of the electronic configuration of $[Rh_2(CH_3COO)_4]$ is closely related to the ratio of the HF exchange potential in the DFT methods.

**Relation between Geometry and Electronic Configuration.** To explain the relation between the geometry and the orbital ordering, we performed UB3LYP calculations of $[Rh_2(CH_3COO)_4]$ with several Rh–Rh lengths. Starting from the optimized geometry, the Rh–Rh length is elongated from 2.36 to 2.56 Å by increments of 0.02 Å. In those calculations, the acetato ligands are fixed. The obtained potential energy surface and the orbital diagrams are shown in Figure 5.

As shown in Figure 5a, an energy minimum appears around 2.38 Å on the Rh–Rh length. This is consistent with the optimized geometry, and other minima are not found within this range. Figure 5b shows that a shorter Rh–Rh length stabilizes the $\sigma$ and $\pi$ orbitals, and unstabilizes the $\sigma^*$ orbital. This phenomenon is easily understood by the change in the orbital overlap. The crossing point between the $\delta$ and $\pi$ orbitals is found around 2.54 Å on the Rh–Rh length, which is 0.16 Å longer than the optimum. However, this value is not realistic in comparison with the optimized or X-ray Rh–Rh length. In other words, a change of Rh–Rh length does not have a large influence on the electronic configuration.

Next, in order to clarify the relation between the electron configuration and the $H_2O$ position, we also carried out UB3LYP calculations with an artificial model structure of $[Rh_2(CH_3COO)_4(H_2O)_2]$, where the Rh–$OH_2$ length is changed. Starting from the X-ray geometry, the Rh–$OH_2$ length was elongated from 2.30 to 2.45 Å by increments of 0.01 Å. In those calculations, the geometry of the $[Rh_2(CH_3COO)_4]$ component is fixed. The obtained potential energy surface, Rh–$OH_2$ binding energy ($\Delta_{bind}$(Rh–$OH_2$)), absolute value of differential energy between $\sigma$ and $\delta$ orbitals, and the orbital diagrams are shown in Figure 6.

As shown in Figure 6a, the energy minima of the total energy and binding energy are found around 2.39 Å on the Rh–Rh length, which is also consistent with the optimized geometry. Other energy minima are not found within this range. Figure 6d shows that the Rh–$OH_2$ length strongly affects the stabilization of the $\sigma$ and $\sigma^*$ orbitals. Interestingly, the orbital energies of the $\sigma$ and $\delta$ orbitals have a crossing point around 2.35 Å. This suggests that the position of $H_2O$ strongly affects the stability of the $\sigma$ orbital, and consequently, the orbital energy order seems to be easily changed.

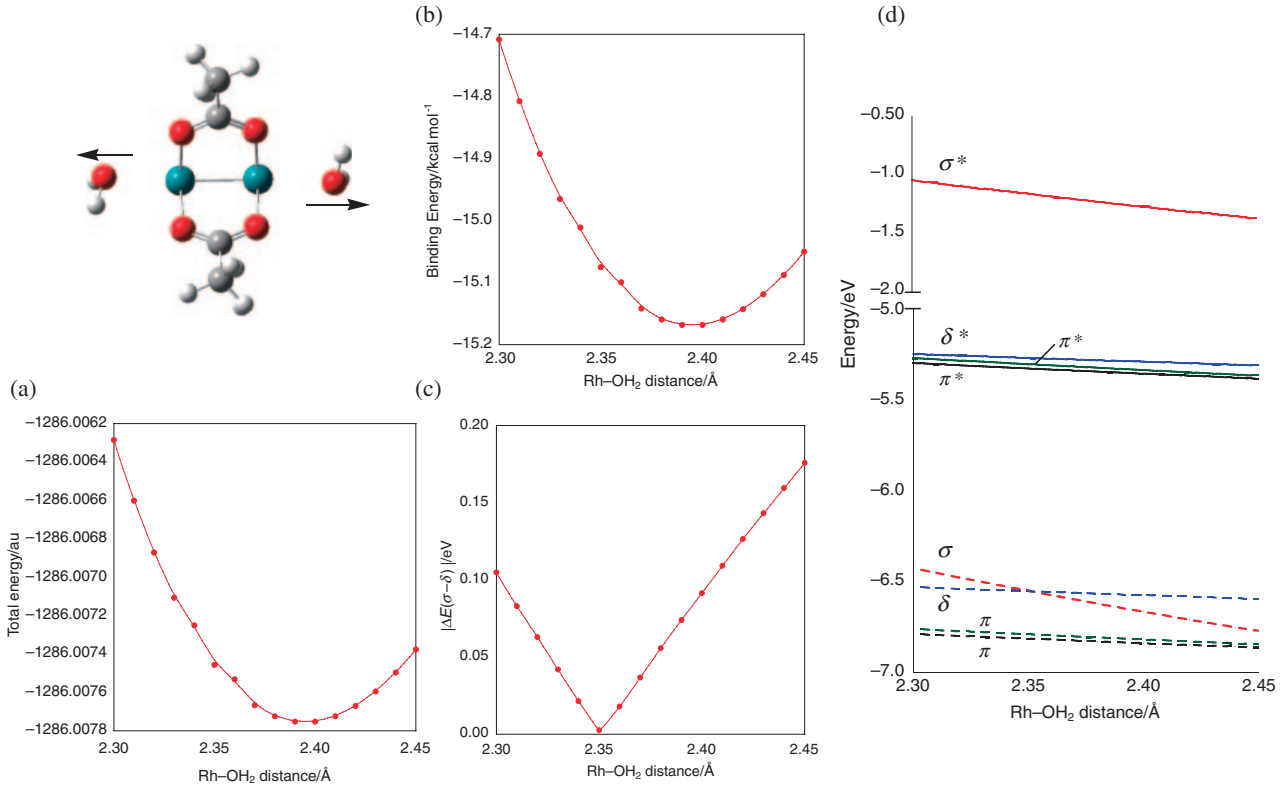


**Figure 6.** UB3LYP calculation of (a) total potential energy surface, (b) $\Delta_{bind}$(Rh–OH$_2$), (c) $|\Delta E(\sigma - \delta)|$, and (d) molecular orbital diagrams dependence on the Rh–OH$_2$ length in $[Rh_2(CH_3COO)_4(H_2O)_2]$.

**Table 5.** $n_i$, $y_i$, and $b_i$ Values of $[Rh_2(CH_3COO)_4(L)_2]$

| Model structure | Functional | Geometry | $n_i$ ($\sigma$) | $n_i$ ($\sigma^*$) | $y_i$ | $b_i$ |
|---|---|---|---|---|---|---|
| $[Rh_2(CH_3COO)_4(H_2O)_2]$ | UHF | X-ray | 1.571 | 0.429 | 13.9 | 0.571 |
| | | Optimize | 1.397 | 0.603 | 31.4 | 0.397 |
| | UBHandHLYP | X-ray | 1.937 | 0.063 | 0.20 | 0.937 |
| | | Optimize | 1.893 | 0.107 | 0.60 | 0.893 |
| | UB3LYP | X-ray | 2.000 | 0.000 | 0.0 | 1.00 |
| | | Optimize | 2.000 | 0.000 | 0.0 | 1.00 |
| | UBLYP | X-ray | 2.000 | 0.000 | 0.0 | 1.00 |
| | | Optimize | 2.000 | 0.000 | 0.0 | 1.00 |
| $[Rh_2(CH_3COO)_4]$ | UHF | Optimize | 1.391 | 0.609 | 32.1 | 0.391 |
| | UBHandHLYP | Optimize | 1.882 | 0.118 | 0.80 | 0.882 |
| | UB3LYP | Optimize | 2.000 | 0.000 | 0.0 | 1.00 |
| | UBLYP | Optimize | 2.000 | 0.000 | 0.0 | 1.00 |

**Nature of the Rh–Rh Bond.** In order to examine the nature of the metal–metal bond between Rh ions, NO analyses were carried out on $[Rh_2(CH_3COO)_4(L)_2]$ (L = none, $H_2O$) complexes. The obtained occupation numbers ($n_i$), instability values ($y_i$), and effective bond orders ($b_i$) are summarized in Table 5.

All the results show that the $\sigma$ and $\sigma^*$ orbitals are the HONO and the LUNO, respectively, and indicate that the Rh–Rh bond is a single bond. In Figure 7, the HONO and LUNO of $[Rh_2(CH_3COO)_4(L)_2]$ calculated by the UB3LYP with the optimized and X-ray geometries are depicted.

The $n_i$ and $y_i$ values of the Rh–Rh single bond calculated by the UB3LYP method are close to 2.0 and 0.0, respectively, showing that the $\sigma$ bond is an almost closed shell type orbital. In other words, a large overlap and a strong interaction exist between the Rh ions.

In the previous section, we suggested that the axial $H_2O$ molecules affected the orbital energies. From these values at each geometry, we found that the change in the $H_2O$ geometry hardly influenced the overlap of the Rh–Rh single bond. For the UBHandHLYP method, the calculated $b_i$ values of the X-ray and optimized geometry are 0.937 and 0.893, respectively, indicating that the instability in the $\sigma$ orbital is caused by the excitation to the $\sigma^*$ orbital. The UHF calculation shows a much smaller $b_i$ value. These results demonstrate that the Rh–Rh overlap becomes smaller with the increase in HF exchange

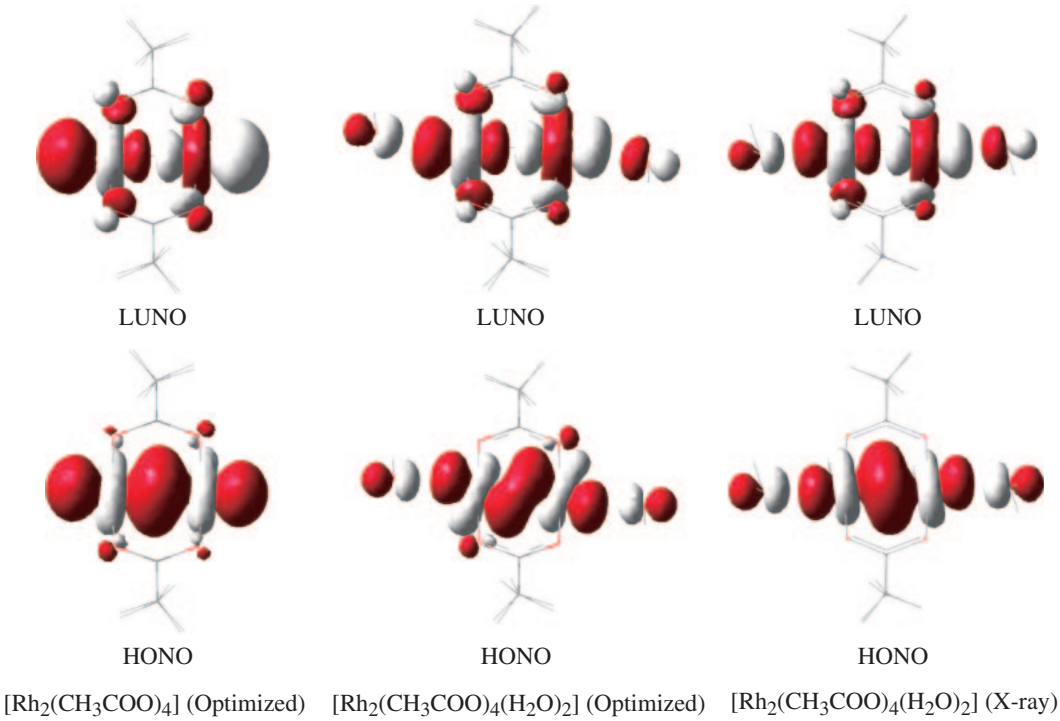


**Figure 7.** Natural orbital of $[Rh_2(CH_3COO)_4(L)_2]$ calculated with UB3LYP functional method.

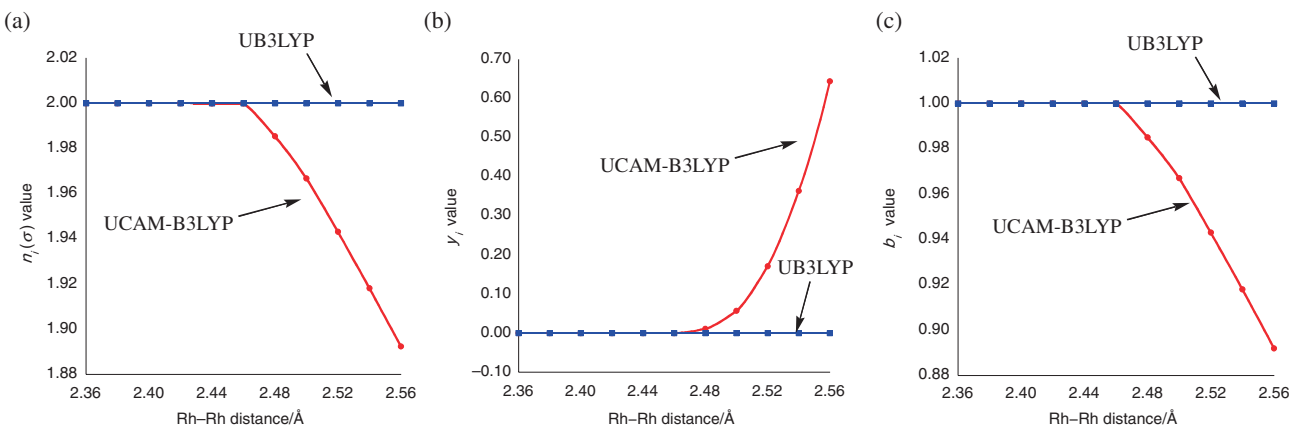


**Figure 8.** $n_i$, $y_i$, and $b_i$ values variation of dependence on Rh–Rh length in $[Rh_2(CH_3COO)_4]$.

potential. The same effects are also found in $[Rh_2(CH_3COO)_4]$.

In order to elucidate the effect of the HF exchange potential, especially for the long-range correlation, we also carried out calculations using the UCAM-B3LYP method.[16] The results for the $n_i$, $y_i$, and $b_i$ values are depicted in Figures 8a–8c, respectively.

As shown in Figure 8, the $n_i$, $y_i$, and $b_i$ values calculated by the UB3LYP method are constant for all the examined Rh–Rh lengths, indicating that the $\sigma$ bond is a closed shell. On the other hand, the UCAM-B3LYP calculation shows instability where the Rh–Rh length is longer than 2.44 Å. From this, it seems that the long-range correlation is important if one must examine longer Rh–Rh interaction.

## Conclusion

In this study, we examined the relation between the electronic configurations (and the orbital ordering), the molecular geometries and the calculation methods in $[Rh_2(CH_3COO)_4(L)_2]$ (L = free, $H_2O$). The calculated results indicate that the electronic configuration is affected by the position of the axial $H_2O$ molecules, but not by the Rh–Rh length. This seems to be the main reason why many electronic configurations have been presented in the past. The DFT functional sets, especially the ratio of the HF exchange, also change the orbital ordering. As illustrated in Figure S1 in the Supporting Information, the HF exchange tends to make the HOMO–LUMO gap longer and the Rh–Rh overlap smaller. Because the decrease of the overlap makes the energy gap between the bonding $\sigma$ and antibonding $\sigma^*$ orbitals smaller, the electronic configurations seem to change along with the enlarged HOMO–LUMO gaps. At this stage, it is difficult to say which functional set is the best for this system but the HF exchange in the exchange-correlation term of the DFT is necessary for the relatively longer Rh–Rh distances. Finally,

we emphasize that the dependency of the orbital ordering on the geometry should be an important factor to consider when examining the photoexcitation of related materials. One must be careful about the ligands on the axial position when considering the photoexcitations.

One of the authors (Y. Kataoka) expresses his special thanks for the Global COE (center of excellence) Program "Global Education and Research Center for Bio-Environmental Chemistry" of Osaka University. This work has been supported by Grants-in-Aid for Scientific Research (KAKENHI) (Nos. 19750046 and 19350070) from Japan Society for the Promotion of Science (JSPS) and that on Grant-in-Aid for Scientific Research on Innovative Areas ("Coordination Programming" area 2170, No. 22108515) from the Ministry of Education, Culture, Sports, Science and Technology (MEXT).

## Supporting Information

The relation between the ratio of the HF exchange potential and the electronic configuration. This material is available free of charge on the web at http://www.csj.jp/journals/bcsj/.

## References

1 a) S. Takamizawa, E. Nakata, H. Yokoyama, K. Mochizuki, W. Mori, *Angew. Chem., Int. Ed.* **2003**, *42*, 4331. b) M. W. Cooke, G. S. Hanan, F. Loiseau, S. Campagna, M. Watanabe, Y. Tanaka, *J. Am. Chem. Soc.* **2007**, *129*, 10479. c) M. Handa, M. Watanabe, D. Yoshioka, S. Kawabata, R. Nukada, M. Mikuriya, H. Azuma, K. Kasuga, *Bull. Chem. Soc. Jpn.* **1999**, *72*, 2681.

2 a) M. Bień, F. P. Pruchnik, A. Seniuk, T. M. Lachowicz, P. Jakimowicz, *J. Inorg. Biochem.* **1999**, *73*, 49. b) F. P. Pruchnik, P. Jakimowicz, Z. Ciunik, J. Zakrzewska-Czerwińska, A. Opolski, J. Wietrzyk, E. Wojdat, *Inorg. Chim. Acta* **2002**, *334*, 59.

3 a) J. Hansen, H. M. L. Davies, *Coord. Chem. Rev.* **2008**, *252*, 545. b) S. Naito, T. Tanibe, E. Saito, T. Miyao, W. Mori, *Chem. Lett.* **2001**, 1178. c) Y. Kataoka, K. Sato, Y. Miyazaki, Y. Suzuki, H. Tanaka, Y. Kitagawa, T. Kawakami, M. Okumura, W. Mori, *Chem. Lett.* **2010**, *39*, 358.

4 F. A. Cotton, B. G. DeBoer, M. D. Laprade, J. R. Pipal, D. A. Ucko, *J. Am. Chem. Soc.* **1970**, *92*, 2926.

5 L. Dubicki, R. L. Martin, *Inorg. Chem.* **1970**, *9*, 673.

6 J. G. Norman, Jr., H. J. Kolari, *J. Am. Chem. Soc.* **1978**, *100*, 791.

7 H. Nakatsuji, J. Ushio, K. Kanda, Y. Onishi, T. Kawamura, T. Yonezawa, *Chem. Phys. Lett.* **1981**, *79*, 299.

8 D. L. Lichtenberger, J. R. Pollard, M. A. Lynn, F. A. Cotton, X. Feng, *J. Am. Chem. Soc.* **2000**, *122*, 3182.

9 O. V. Sizova, N. V. Ivanova, *Russ. J. Coord. Chem.* **2006**, *32*, 444.

10 a) J. Lloret, J. J. Carbó, C. Bo, A. Lledós, J. Pérez-Prieto, *Organometallics* **2008**, *27*, 2873. b) G. G. Christoph, Y. B. Koh, *J. Am. Chem. Soc.* **1979**, *101*, 1422. c) A. L. Sargent, M. E. Rollog, C. T. Eagle, *Theor. Chem. Acc.* **1997**, *97*, 283, and their references.

11 a) E. Nakamura, N. Yoshikai, M. Yamanaka, *J. Am. Chem. Soc.* **2002**, *124*, 7181. b) G. Costantino, R. Rovito, A. Macchiarulo, R. Pellicciari, *THEOCHEM* **2002**, *581*, 111.

12 a) M. J. Frisch, G. W. Trucks, H. B. Schlegel, G. E. Scuseria, M. A. Robb, J. R. Cheeseman, J. A. Montgomery, Jr., T. Vreven, K. N. Kudin, J. C. Burant, J. M. Millam, S. S. Iyengar, J. Tomasi, V. Barone, B. Mennucci, M. Cossi, G. Scalmani, N. Rega, G. A. Petersson, H. Nakatsuji, M. Hada, M. Ehara, K. Toyota, R. Fukuda, J. Hasegawa, M. Ishida, T. Nakajima, Y. Honda, O. Kitao, H. Nakai, M. Klene, X. Li, J. E. Knox, H. P. Hratchian, J. B. Cross, V. Bakken, C. Adamo, J. Jaramillo, R. Gomperts, R. E. Stratmann, O. Yazyev, A. J. Austin, R. Cammi, C. Pomelli, J. W. Ochterski, P. Y. Ayala, K. Morokuma, G. A. Voth, P. Salvador, J. J. Dannenberg, V. G. Zakrzewski, S. Dapprich, A. D. Daniels, M. C. Strain, O. Farkas, D. K. Malick, A. D. Rabuck, K. Raghavachari, J. B. Foresman, J. V. Ortiz, Q. Cui, A. G. Baboul, S. Clifford, J. Cioslowski, B. B. Stefanov, G. Liu, A. Liashenko, P. Piskorz, I. Komaromi, R. L. Martin, D. J. Fox, T. Keith, M. A. Al-Laham, C. Y. Peng, A. Nanayakkara, M. Challacombe, P. M. W. Gill, B. Johnson, W. Chen, M. W. Wong, C. Gonzalez, J. A. Pople, *Gaussian 03, Revision D.02*, Gaussian, Inc., Wallingford CT, **2004**. b) M. J. Frisch, G. W. Trucks, H. B. Schlegel, G. E. Scuseria, M. A. Robb, J. R. Cheeseman, G. Scalmani, V. Barone, B. Mennucci, G. A. Petersson, H. Nakatsuji, M. Caricato, X. Li, H. P. Hratchian, A. F. Izmaylov, J. Bloino, G. Zheng, J. L. Sonnenberg, M. Hada, M. Ehara, K. Toyota, R. Fukuda, J. Hasegawa, M. Ishida, T. Nakajima, Y. Honda, O. Kitao, H. Nakai, T. Vreven, J. A. Montgomery, Jr., J. E. Peralta, F. Ogliaro, M. Bearpark, J. J. Heyd, E. Brothers, K. N. Kudin, V. N. Staroverov, R. Kobayashi, J. Normand, K. Raghavachari, A. Rendell, J. C. Burant, S. S. Iyengar, J. Tomasi, M. Cossi, N. Rega, J. M. Millam, M. Klene, J. E. Knox, J. B. Cross, V. Bakken, C. Adamo, J. Jaramillo, R. Gomperts, R. E. Stratmann, O. Yazyev, A. J. Austin, R. Cammi, C. Pomelli, J. W. Ochterski, R. L. Martin, K. Morokuma, V. G. Zakrzewski, G. A. Voth, P. Salvador, J. J. Dannenberg, S. Dapprich, A. D. Daniels, Ö. Farkas, J. B. Foresman, J. V. Ortiz, J. Cioslowski, D. J. Fox, *Gaussian 09, Revision A.1*, Gaussian, Inc., Wallingford CT, **2009**.

13 a) K. Yamaguchi, T. Kawakami, Y. Takano, Y. Kitagawa, Y. Yamashita, H. Fujita, *Int. J. Quantum Chem.* **2002**, *90*, 370. b) Y. Kitagawa, M. Shoji, K. Koizumi, T. Kawakami, M. Okumura, K. Yamaguchi, *Polyhedron* **2007**, *26*, 2154. c) M. Shoji, K. Koizumi, Y. Kitagawa, S. Yamanaka, M. Okumura, K. Yamaguchi, Y. Ohki, Y. Sunada, M. Honda, K. Tatsumi, *Int. J. Quantum Chem.* **2006**, *106*, 3288.

14 a) K. Takatsuka, T. Fueno, K. Yamaguchi, *Theor. Chim. Acta* **1978**, *48*, 175. b) K. Yamaguchi, M. Okumura, K. Takada, S. Yamanaka, *Int. J. Quantum Chem.* **1993**, *48*, 501.

15 K. Andersson, C. W. Bauschlicher, Jr., B. J. Persson, B. O. Roos, *Chem. Phys. Lett.* **1996**, *257*, 238.

16 T. Yanai, D. P. Tew, N. C. Handy, *Chem. Phys. Lett.* **2004**, *393*, 51.